


Automated Parametric Optimization of a High-Purity Germanium Monte Carlo Neutral-Particle Model (December 2017)

Bryan V. Egner, *Student, AFIT*, Robert S. Torzilli, *Student, AFIT*

Abstract—High-purity germanium detector Monte Carlo Neutral-Particle (MCNP) models can be created, and then optimized using an automated parametric optimization code to resemble experimental data. Developing an MCNP model of a HPGe detector solely off manufacturer provided information is not sufficient. Matching simulated data to experimental data requires an understanding of radiation transport both in reality and in a simulated environment as well as knowledge of the internal detector components with their potential uncertainties. Literature often neglects to inform readers about the development of such models, and the difficulties faced in optimizing parameters. The methodology used to match MCNP calculated efficiencies of a HPGe detector to experimental data was to develop a base model where various parameters could be optimized in a brute-force manner using a generic automated code. This requires the user to only have knowledge of how MCNP works, and a schematic diagram of the detector. The results showed that this method can create efficiency curves as a function of incident photon energies above 159 keV, with a maximum relative difference of less than 5.9%. 

Index Terms— Absolute Efficiency, Gamma-Ray Spectroscopy, HPGe, MCNP, Parametric Optimization


I. INTRODUCTION

Gamma-ray spectroscopy using HPGe detectors is a leading method for obtaining high-energy resolution spectra in both the laboratory setting and in the field. These detectors have the ability to obtain energy resolutions as low as 0.15 keV for the Full-Width-Half-Maximum, at incident photons around 5.9 keV. [1] The tradeoff for such high energy resolution is an overall lower detection efficiency compared to other types of nuclear instrumentation; such as sodium iodide, NaI, scintillators. The advancement of radiation transport codes, such as MCNP, allows researchers to accurately model the detection response of HPGe detectors at various geometries, source energies, and environments. Radiation transport modeling provides insight to potential anomalies that could occur during an experiment and enables the user to intelligently modify experiments which could improve results, conserve resources, and ensure safety requirements are followed. Unfortunately, creating a detector MCNP model that accurately

represents reality can be difficult and time consuming. By applying a systematic or computational approach, this process can be streamlined. Rather than manually performing trial-and-error adjustments to match experimental data, the development of an automated parametric optimization code will simplify the enhancement of a rudimentary HPGe detector model. Ideally, an optimized HPGe MCNP model should accurately predict the detection efficiency curves at various source positions which can then be applied to developing an adjoint flux model representing the detection efficiency over all space.

II. PROBLEM DESCRIPTION

The development of an MCNP model that accurately resembles a detector's experimental response is not an elementary task. Factors to consider when modeling are: the type and position of the radiation source, the properties, both geometrical and composition of the detector being modeled, and the characteristics of primary and secondary incident radiation. Published literature has stated relative differences between the experimental and Monte Carlo simulated full-energy peak absolute efficiencies for HPGe detectors have reached as low as 0.2%. [2] There have also been studies showing discrepancies between the manufacturer provided detector specifications of internal components compared to measured values, such as the crystal length and dead layers. [3]

Experimental measurements of gamma-ray emissions using a standard Canberra p-type HPGe detector were provided by Lieutenant Colonel Buckley O'Day using a multi-nuclide source. The multi-nuclide source covered photon energies ranging from 0.06 to 1.836 MeV, which allowed for a full representation of the absolute efficiency curve. The numerical values listed for the energies in Table 1 follow the rounding format listed on the source specifications sheet provided by Eckert & Ziegler Isotope Products. The documentation also states the source uncertainty to be 3.1% for each energy. 

B. V. Egner is with the Engineering Physics Department at the Air Force Institute of Technology, Wright Patterson AFB, OH 45431 (e-mail: bryan.egner@afit.edu, phone: (717)736-3846).

R.Torzilli is with the Engineering Physics Department at the Air Force Institute of Technology, Wright Patterson AFB, OH 45431 (e-mail: robert.torzilli@afit.edu).

TABLE 1
MULTI-NUCLIDE SOURCE INFORMATION

Gamma-Ray Energy [keV]	Nuclide	Activity [μCi]	Gammas per Second
60	Am-241	0.02941	391.7
88	Cd-109	0.2707	363.6
122	Co-57	0.01019	322.7
159	Te-123	0.01403	436.1
320	Cr-51	0.3389	1236
392	Sn-113	0.05109	1227
514	Sr-85	0.06171	2247
662	Cs-137	0.04325	1362
898	Y-88	0.09633	3347
1173	Co-60	0.05101	1885
1333	Co-60	0.05101	1887
1836	Y-88	0.09622	3539

A labeled diagram of the various source positions with respect to the HPGe detector are shown in Figure 2. At each position, a 24-hour count was performed to minimize uncertainty. For position 1, the source was placed centered on the Al casing, position 2 was resting on the front face and flush with the edge of the casing, position 3 was centered 7 cm above the front face, position 4 was placed 3 cm down the side of the casing, and position 5 was offset 13 cm above the detector.

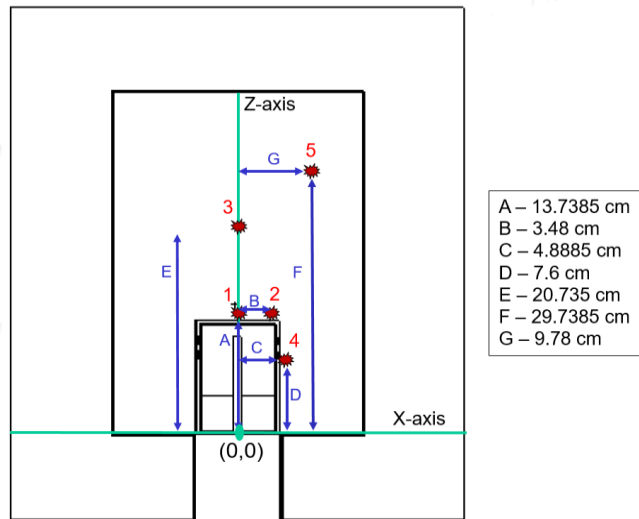


Fig. 1. Experimental setup diagram displaying each source position on a Cartesian coordinate system. The origin is centered at the base of the Al casing of the detector.

A plot of the spectra and the calculated absolute efficiencies as a function of energy were also provided by Lt Col O'day for comparison with the simulated results. The absolute efficiency was calculated using Equation 1.

$$\varepsilon_{abs} = \frac{N_c}{A_g * t_l * \exp\left[-\frac{\ln 2}{t_{1/2}} * t_d\right]} \quad \text{Equation 1}$$

N_c is the total number of counts under the full-energy peak. A_g is the amount of gammas emitted per second which is listed in column 4 of Table 1, multiplied by the live time, t_l , in seconds.

The source decay is accounted for by multiplying the denominator by the decay exponential where $t_{1/2}$ is the half-life, and t_d is the age of the source both in seconds.

III. DESCRIPTION OF WORK

First, a HPGe detector model was created using MCNP, and then an optimization code was produced in Python. After the model was optimized, efficiency curves were plotted for quantitative analysis, then ADVANTG weight windows were implemented to generate the adjoint flux response for a qualitative representation of the results.

A. HPGe MCNP Model

The MCNP model was designed based off the manufacturer provided detector diagram labeling various dimensions and materials. Unfortunately, some dimensions were not labeled, including information about the internal contact pin, gap widths between the Ge crystal and the inner Al holder, and the insulation materials. For higher energy photons, these features are not as important, but for the lower energies, attenuation is more probable to occur which might affect the results. Knowing that the overall goal of the generic MCNP model was to have easily adjustable parameters, the decision was made to only use right circular cylinders and planes. This would allow the model to be easily adjusted where the only changes needed to be made would be raising or lowering the heights, and widening or compressing the widths. The final design of the generic HPGe MCNP model generated in VisEd is illustrated in Figure 2.

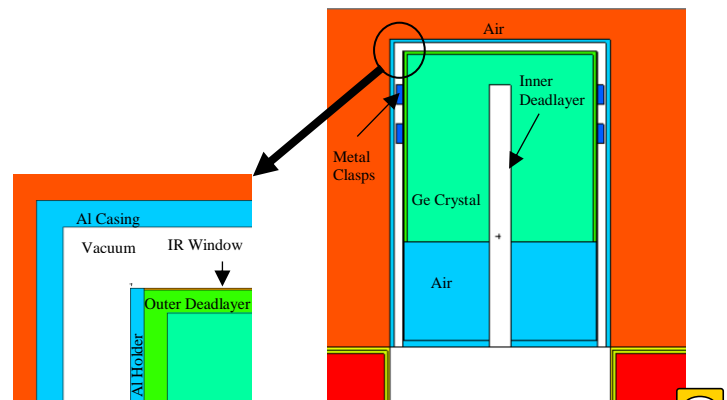


Fig. 2. Generic HPGe Model displayed using VisEd. An enlarged view of the top edge of the Ge crystal is shown, where the IR window is placed on the top of the outer deadlayer, flush with the top of the Al holder.

The IR window placed directly above the top deadlayer is composed of a thin 0.01016 cm Kapton tape window and a 0.000847 cm Al Mylar layer. Both the Ge crystal top edges and the top of the inner coaxial were assumed to be squared, rather than rounded, since the manufacture did not specify these features. In the left image of Figure 2, the outer deadlayer can be seen and it was assumed to be a lithium drifted surface. The inner deadlayer contact was assumed to be a boron implanted contact. Neither of these materials were explicitly stated in the detector schematic, and the compositional assumptions were

based on previous knowledge of p-type HPGe detectors. [1] The materials used for other components in the MCNP model were standard for HPGe detectors and a full list can be found in Table 2. All material composition data was found in Los Alamos National Laboratory's ACE Data Tables or Pacific North Western National Laboratory's Compendium of Material Composition Data for Radiation Transport Models [4] [5] The cross-sectional data library used was mcplib84p) for photon transport which was composed of 278 energy groups.

TABLE 2
MCNP MATERIAL COMPOSITIONS

Material	Density [g/cm ³]	Component(s)
Mylar	1.38	IR Window
Brass	8.41	Metal Clasps
Aluminum	2.7	Detector Housing and Casing
Germanium	5.32	Ge Crystal
Lithium	0.534	Outer Deadlayer
Boron	2.73	Inner Deadlayer
Copper	8.96	Shield Lining
Tin	7.31	Shield Lining
Kapton Film	1.42	IR Window
Air	0.001224	Shielding Chamber
Lead	11.34	Shielding
Acrylic Glass	1.19	Source Encapsulation
Vacuum	---	Coaxial Space

The ~~Data Block~~ of the MCNP model also consisted of information about the photon transport, physics, tallies and the source definition. Only photons were tracked in the simulation because only the absolute efficiency was desired. Therefore, a full energy spectrum that accounts for secondary radiation was not required and the Gaussian Energy Broadening Card was not utilized. The default Physics Card settings were used, which means Bremsstrahlung, coherent scattering, and photo-fission were ignored. The source card created an isotropic point source that emitted 12 discrete photon energies, each with the same probability distribution. The actual energies are displayed in Table 1. The energy deposition, F8, tally was used to track each particle's interaction with the Ge crystal, and 10⁶ source particles were used to reduce uncertainties.

After the model was created, research to which parameters have the largest effect on a HPGe detection efficiency was performed and it was found that the deadlayers, entrance windows, the Ge crystal length and radius played the largest role in photon attenuation. [2] Understanding that lower energy photons will be more affected by attenuating layers between the source and physical Ge crystal, and that higher energy photon interactions depend more on the length and radius of the crystal, a list of the parameters that were optimized can be found in Table 3.

TABLE 3
HPGE MCNP MODEL PARAMETERS TO OPTIMIZE

Parameter	Initial Value	Lower Bound	Upper Bound
Outer Top Deadlayer [cm]	0.13	0.013	73899333
Outer Sides Deadlayer [cm]	0.13	0.03	0.23
Ge Crystal Length [cm]	8.32	7.474993997	9.165002
Kapton Window [cm]	0.010	0.00516	0.11016

Inner Top Coaxial Deadlayer [cm]	3.00E-05	5.67E-06	0.00013
Inner Sides Coaxial Deadlayer [cm]	3.00E-05	1.00E-05	1.00E-04
Top Al Casing Thickness [cm]	0.15	0.05	0.25
Sides Al Casing Thickness [cm]	0.15	0.05	0.25
Ge Crystal Density [g/cm]	5.32	5.29	5.32

B. Automated Parametric Optimization Code

The Automated Optimizer for MCNP Input Decks, hence forth referred to as the application, uses User supplied data, points of interest, parameters of interest, and a prepared MCNP input deck in an attempt to create an experimentally observed detector. It accomplishes this task by iterating through all defined points for each parameter and keeps the ones that minimize the chi squared value, Equation 2. Once it has determined this is the best value it can achieve from the iterations, it moves on to the next parameter and repeats this process.

$$\chi^2 = \sum_{i=0}^N \frac{(D_a - D_e)^2}{\sigma^2} \quad \text{Equation 2}$$

Where χ^2 , chi squared, is equal to the sum over all the data points of interest, D_a is the analytical derived point created by the application, D_e is the captured experimental data that the application is trying to match, and σ is the uncertainty of that experimental data. The closer chi squared is to one, the better fit it is to the experimental data.

The application's secondary purpose is to automate the collection of relevant data for the purpose of recording what other parameters could be of interest based on how it affects the overall data. This is accomplished by printing out the relative error, Equation 3, the average error, Equation 4, and plots of the data superimposed upon the experimental data in an easy to read format.


$$E = \frac{|D_a - D_e|}{|D_e|} \quad \text{Equation 3}$$

$$\bar{E} = \frac{\sum_{i=0}^N E}{N} \quad \text{Equation 4}$$

Where E is the relative error of each pair of points, \bar{E} is the mean of the relative error, and N is the total number of relative error points that were calculated.

To put it simply this application reads through the MCNP output file to retrieve the wanted information and stores it a more readable fashion. From these outputs, the User can determine if an interested parameter is behaving as expected or if it even affects the model in a meaningful way. This should make it easier to determine what values need to be adjusted as well as what could be occurring to cause a difference in the model versus the experiment. An example of this will be discussed in the next section.

For a list of current assumptions, how to change it to work with other detectors, as well as a more detailed outline of how

the application works, see the User Manual. 

IV. RESULTS

Five efficiency curves were produced from the output of the F8 tallies and the results are shown in Figures 3 through 7. Due to a potential error in the experimental data provided the Cr-51, 320 keV efficiency was neglected and only 11 energies were plotted. Figure 3 displays the experimental and MCNP absolute efficiencies for source position 1 where the average relative difference was 52%, and the minimum relative difference was 2%. The experimental and MCNP results match up fairly well for energies above 159 keV, but the lower energies have 100% or more, relative differences.

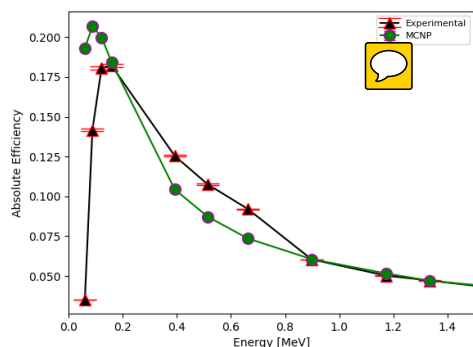


Fig. 3. Experimental and MCNP absolute efficiency as a function of photon energy at position 1, centered on the Al end cap.

The results for position 2, displayed in Figure 4, showed a similar behavior as position 1; where the experimental efficiencies for lower energy photons varied drastically compared to the MCNP model. The average relative difference was slightly better, 47.8%.

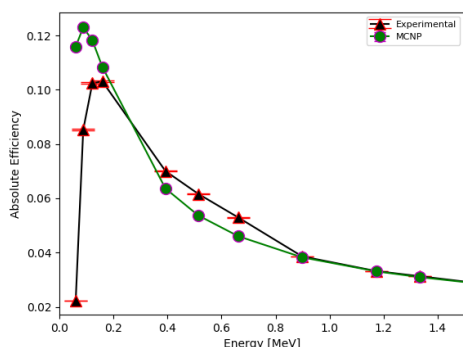


Fig. 4. Experimental and MCNP absolute efficiency as a function of photon energy at position where the source is resting on the endcap, flush with the outer edge.

In Figure 5, the results showed a larger variance at lower energies, but following the same trend matched the higher energies better.

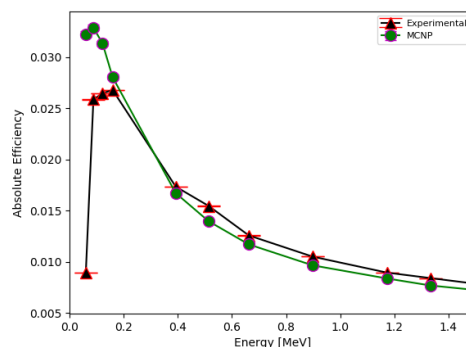


Fig. 5. Experimental and MCNP absolute efficiency as a function of photon energy at position 3, centered and 7 cm above the Al end cap.

When the source was placed on the side of the HPGe detector, the experimental and MCNP efficiencies were not in agreement with an average relative difference of 452%, as shown in Figure 6.

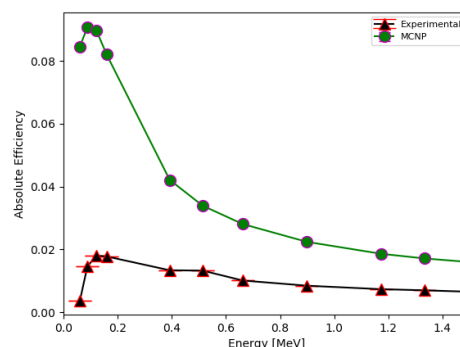


Fig. 6. Experimental and MCNP absolute efficiency as a function of photon energy at position 4, 6 inches down the side of the Al casing.

The results for the final position for a source offset and 13 cm above the detector had a similar efficiency curve shape to positions 1, 2, and 3, as shown in Figure 7. Comparing all five positions, it is evident that there is a lot more photon attenuation in the experimental data compared to what is occurring in the MCNP model.

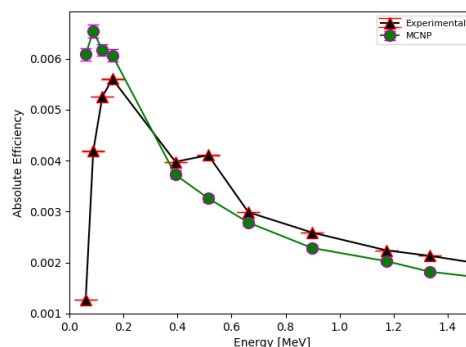


Fig. 7. Experimental and MCNP absolute efficiency as a function of photon energy at position 5, offset 13 cm above the detector.

Chi squared was introduced but not used in the analysis - no chi squared results reported.

It is worth noting that the simulated shapes make a lot of sense to me whereas the experimental data doesn't always. That said, I have not taken data with this particular detector in a long time...

After running through all combinations, the final parameters outputted by the automated optimization code can be found in Table 4. Most of the adjustments for each source position were

similar, where the top deadlayer was increased and the crystal length was shortened.

TABLE 4
OPTIMIZED DETECTOR PARAMETERS

Parameter	Initial Value	1	2	Position: 3	4	
Outer Top Deadlayer [cm]	0.13	0.7389	0.7389	0.7389	0.7389	
Outer Sides Deadlayer [cm]	0.13	0.23	0.23	0.23	1.35	0.23
Ge Crystal Length [cm]	8.32	7.6627	7.4749	7.4749	7.4749	7.4749
Kapton Window [cm]	0.010	0.1101	0.1101	0.1101	0.0576	0.1101
Inner Top Coaxial Deadlayer [cm]	3E-05	0.0001	6E-05	6E-05	0.0001	6E-05
Inner Sides Coaxial Deadlayer [cm]	3E-05	2E-05	6E-05	7E-05	0.001	7E-05
Top Al Casing Thickness [cm]	0.15	0.25	0.25	0.25	0.05	0.25
Sides Al Casing Thickness [cm]	0.15	0.05	0.05	0.05	0.27	0.25
Ge Crystal Density [g/cm ³]	5.32	5.32	5.32	5.35	5.32	5.3425

After outputting the results and examining a consistent trend, where the efficiency curves matched well at higher energies but poorly at energies below 159 keV, another optimization trial was performed at position 3. For this case, the optimization code neglected all energies below 159 keV and the results can be seen in Figure 8 and Table 5. A stronger agreement was found between experimental and MCNP calculated efficiencies where the average relative difference was 2.4 %. Also, the range for the top deadlayer was increased to cause more photon attenuation and potentially provide better results.

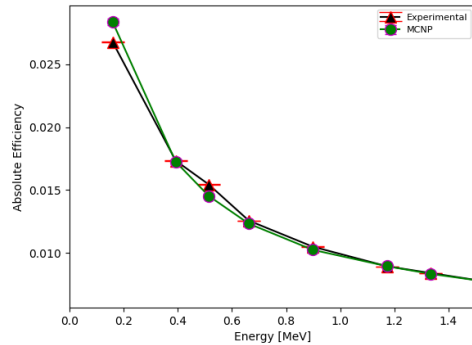


Fig. 8. Experimental and MCNP absolute efficiency as a function of photon energy at position 3 for energies 159 keV and higher.

TABLE 5
OPTIMIZED DETECTOR PARAMETERS FOR POSITION 3

Parameter	Initial Value	Position 3	Position 3 Adjusted
Outer Top Deadlayer [cm]	0.13	0.73899	0.97535
Outer Sides Deadlayer [cm]	0.13	0.23	0.13
Ge Crystal Length [cm]	8.32	7.47499	8.60166
Kapton Window [cm]	0.0101	0.11016	0.13016
Inner Top Coaxial Deadlayer [cm]	0.00003	6E-05	50E-05
Inner Sides Coaxial Deadlayer [cm]	0.00003	7E-05	5E-05
Top Al Casing Thickness [cm]	0.15	0.25	0.18333

Sides Al Casing Thickness [cm]	0.15	0.05	0.25
Ge Crystal Density [g/cm ³]	5.32	5.35	5.35

Using the optimized position 3 MCNP input deck where photon energies below 159 keV were neglected, an adjoint flux contour plot was generated using ADVANTG and VisIT. Figure 9 represents the integral adjoint flux over all photon energies, thus representing the detectors adjoint response. From the adjoint flux response, it is evident that a photon is less likely to be absorbed near edges and above the coaxial.

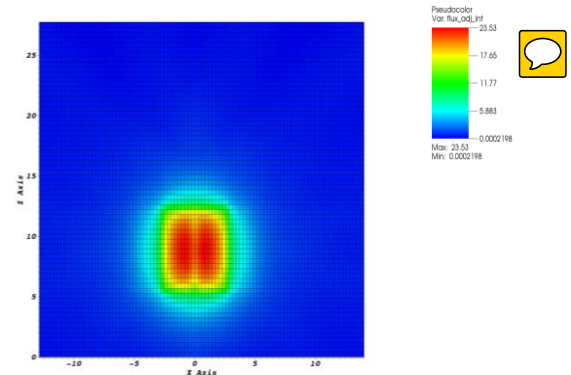


Fig. 9. Adjoint photon flux generated from the optimized detector configuration for a source at position 3. The plot was generated using ADVANTG and edited in VisIt.

V. CONCLUSION

The automated parametric optimization method was able to produce a HPGe MCNP model that can represent the absolute efficiency between energies of 159 keV to 1.836 MeV, with a relative difference less than 5.9% for sources placed 7 cm above the detector. Most likely, the method can also produce similar results for a source farther away. Areas where the method failed to resemble experimentally obtained efficiencies are at low photon energies and locations where there would be internal components holding the Ge crystal in place, such as source positions 2 and 4. Regions that have more attenuation layers will also have more secondary radiation produced, which was not accounted for in this model. There are potentially abnormalities in the provided experimental data itself, and so more measurements should be taken. However, this should be done with single monenergetic sources, not a multi-nuclide source, in order to minimize coincident interactions between different photon energies, escape peaks, and Compton continuum interferences.

The results also show that a better understanding of how to model lower energy photons in MCNP is required. This means a more detailed description of the internal components is essential as well as performing X-ray scans of the detector if the manufacturer is unable to provide a more detailed schematic. The optimization method does not account for impossible dimensions, other than ensuring layers do not overlap. By having X-ray scans, more precise dimensions can be used in the base model allowing for a better comparison of the differences in radiation transport in MCNP and reality.

In the future, more adjustable parameters will be added to the optimization code along with more realistic radiation transport physics to be able to reproduce experimental spectra. Efforts might be made to generalize the structure of the automation optimization code to be applicable for other detectors and experiments, as well as further exploration into alternative means of optimization.

ACKNOWLEDGMENT

We are grateful for the inspiration and mentorship of Captain James Bevins (AFIT/ENP), whom taught NENG 685 during the fall 2018 Quarter at the Air Force Institute of Technology (AFIT). We are appreciative of Lt Col O'Day (AFIT/ENP) for providing experimental data, and Mr. Will Kable (LLNL) and Capt Bevins for providing a template HPGe MCNP model and a template for running ADVANTG.

REFERENCES

- [1] G. F. Knoll, Radiation Detection and Measurement, Hoboken, NJ: John Wiley & Sons, Inc., 2010.
- [2] R. G. Helmer, R. G. Hardy, V. E. Jacob, M. Sanchez-Vega, R. G. Neilson and J. Nelson, "The use of Monte Carlo Calculations in the Determination of a Ge Detector Efficiency Curve," *Nuclear Instruments and Methods in Physics Research*, vol. 551, no. A, pp. 360-381, 2002.
- [3] R. M. Keyser, "Resolution and Sensitivity as a Function of Energy and incident Geometry for Germanium Detectors," *Nuclear Instruments and Methods in Physics Research Section B: Beam Interactions with Materials and Atoms*, vol. 213, pp. 236-240, 2004.
- [4] D. K. P. S. J. G. M. J. L. Conlin, "Listing of Available ACE Data Tables," Los Alamos National Laboratory, Los Alamos National Laboratory, 2013.
- [5] R. McConn, "Compendium of Material Composition Data for Radiation Transport Modeling," Pacific North Western National Laboratory, Richland, WA, 2011.
- [6] R. M. Keyser, "Resolution and Sensitivity as a Function of Energy and incident Geometry for Germanium Detectors," *Nuclear Instruments and Methods in Physics Research Section B: Beam Interactions with Materials and Atoms*, vol. 213, pp. 236-240, 2004.
- [7] S. Guilherme and J. d. S. Corrêa, "COMPUTATIONAL MODELING OF A HIGH PURITY GERMANIUM," in *International Nuclear Atlantic Conference*, Belo Horizonte, MG, Brazil, 2011.
- [8] J. K. Shultis and R. E. Faw, "An MCNP Primer," Department of Mechanical and Nuclear Engineering, Manhattan, KS, 2011.
- [9] D. B. Pelowitz, "MCNP6 User's Manual Version 1.0," Los Alamos National Laboratory, Los Alamos National Laboratory, 2013.